Measurement of the total neutron cross section on argon in the energy range 30 to 70 keV

S. Andringa,[1] Y.Bezawada,[2] T. Erjavec,[2] J. He,[2] J. Huang,[2] P. Koehler,[3] M. Mocko,[3] M. Mulhearn,[2] L. Pagani,[2] E. Pantic,[2] L. Pickard,[2] R. Svoboda,[2] J. Ullmann,[3] and J. Wang[2,4]

(ARTIE Collaboration)

[1] *Laboratório de Instrumentação e Física Experimental de Partículas (LIP), Av. Prof. Gama Pinto, 2, 1649-003, Lisboa, Portugal*

[2] *University of California at Davis, Department of Physics, Davis, CA 95616, U.S.A.*

[3] *Los Alamos National Laboratory, LANSCE, Los Alamos, NM 87545, U.S.A.*

[4] *South Dakota School of Mines and Technology, Physics Department, Rapid City, SD 57701 USA*

(Dated: May 25, 2021)

The cross section for neutron interactions on argon is an important design and operational parameter for a number of neutrino, dark matter, and neutrinoless double beta decay experiments which feature liquid argon as a detection or shielding medium. There is a lingering discrepancy between the total cross section in the 30 to 70 keV neutron kinetic energy region given in the Evaluated Nuclear Data File (ENDF) and the single measurement conducted in the 1990's by an experiment optimized for higher energy. This discrepancy is significant in that the former predicts a large negative resonance in the region while the measurement did not report such a feature, giving rise to significant uncertainty in the interaction length of neutrons in liquid argon. This paper presents results from the Argon Resonant Transport Interaction Experiment (ARTIE) at the Los Alamos Neutron Science Center (LANSCE), the first dedicated experiment optimized for this energy region. The ARTIE measurement of the total cross section as a function of energy confirms the existence of a negative resonance in this region.

INTRODUCTION

Argon is used in a wide range of particle physics experiments investigating neutrinos [1–4], dark matter [5, 19], and neutrinoless double beta decay [6, 7]. Achieving many of the scientific objectives sought by these experiments relies on understanding the transport of neutrons through liquid argon at a level of precision which has only recently emerged as a critical experimental requirement. A recent measurement of the neutron capture cross section [20, 21] settled a roughly 50% discrepancy between previous measurements in favor of the ENDF cross sections[24] for neutron kinetic energy below 1 eV.

The neutron-argon total cross section as predicted by ENDF features an anti-resonance feature at 57 keV which increases the neutron interaction length in liquid argon, for a natural abundance of isotopes, to 42 m. At this energy scale, neutrons only lose a fraction of their kinetic energy during each elastic collision with a relatively massive argon nuclei, and so even neutrons with kinetic energy well above 57 keV eventually reach the anti-resonance feature and the resulting long interation length. The results of the most recent previous measurement [22] were inconsistent with ENDF in the region of the anti-resonance feature, with an inferred interaction length of 6 m. The discrepancy makes it impossible to reliably predict the effectiveness of fiducial volume cuts in liquid argon to suppress neutrons from outside of the detector. In large TPCs like DUNE, neutrons from neutrino interactions will escape the detector volume at an unknown rate, which might impact the energy resolution. The design of calibration systems which use externally produced neutrons relies critically on the precise depth of the anti-resonance feature. This paper describes the Argon Resonance Transport Interaction Experiment (ARTIE) which was designed for the sole purpose of resolving the discrepancy.

ARTIE features an experimental determination of the transmission coefficient T, defined as the fraction of neutrons which pass through a custom liquid argon target without scattering. For a target of length d with atomic number density n_{trg}, the cross section is given by:

$$\sigma = -\frac{1}{n_{\mathrm{trg}}\, d} \ln T. \tag{1}$$

The target thickness $n_{\mathrm{trg}}d$ is a critical experimental parameter, and the ARTIE target was designed to have a thickness approximately twenty times larger than Ref. [22], which casts the cross section discrepancy as competing predictions for transmission coefficient for the ARTIE target of either X or Y. The ARTIE target is well suited to the anti-resonance region, but quickly becomes opaque to neutrons at higher cross section. Our energy region of interest is defined as 30 to 70 keV.

EXPERIMENTAL METHODS

The ARTIE target is a column of liquid argon with a length of 168 cm and a diameter of 25 mm, held at atmospheric pressure, and contained in a vessel constructed from commercial components. For transparency to neu-

trons, the ends of the target were fashioned from kapton foil compressed against a teflon seal in a standard commercial flange. The kapton foil was flushed with gaseous dry nitrogen continuously during operation to minimize ice formation.

The target was inserted into Flight Path 13 (FP13) of the Lujan Neutron Scattering Center [8] at a distance 31 m from the upper-tier liquid hydrogen moderator of the accelerator-driven pulsed neutron source. The Mark III Target-Moderator-Reflector-Shield (TMRS) [25] is driven by an 800 MeV proton linac that produces a 250 ns triangular pulse at a repetition rate of 20 Hz and a typical beam current of 80 μA. Neutrons are produced via spallation reactions inside a tungsten target with a $1/E$ energy spectrum. During data taking, the proton beam current as measured by a current transformer (CT) sensor is recorded once per minute.

The flight path includes a neutron detector, located approximately 30 m downstream of the target, consisting of a 9 cm diameter by 1 mm thick ^{6}Li-glass scintillator, viewed edge-on by two Burle 8854 five-inch photomultiplier tubes (PMTs). We define a neutron event as a pulse above a fixed threshold in ether PMT. The data acquisition system records a timestamp and integrated charge for several time intervals for each neutron event. Describe relationship between timestamp and measured TOF.

Three-inch thick cylindrical blocks of brass with 6 mm holes in the center were used to collimate the beam near the target. Two such collimators were located upstream of the target, and two downstream. When aligned, the collimators constrain the beam to the interior of the 25 mm diameter target, and produce a beam spot with an 8 cm diameter at the 9 cm diameter neutron detector. The final alignment of the collimators was based on beam profile images obtained from storage-phosphor image plates placed at the ^{6}Li detector. Following several iterations, a symmetric image was obtained and the neutron event rate reached a plateau.

For a cost effective design, the ARTIE target uses rigid foam insulation designed for cryogenic applications. Near each ends of the target vessel, an opening upward feeds into a commerical plastic dewar. As argon boils in the detector, gaseous argon vents through the openings and is replaced by liquid argon from the dewars. During normal operation, the dewars were refilled remotely about once per hour to ensure that the target remained full.

The ARTIE experiment collected data during a two week period beginning in October 2019, with most of the data taken in either of two target configurations. During target-in runs, the target vessel was filled with liquid argon (LAr). During target-out runs, the target vessel was continuously flushed with gaseous argon (GAr). The transmission coefficient is experimentally determined as:

$$T = \frac{N_{\text{in}} - B_{\text{in}}}{N_{\text{out}} - B_{\text{out}}} \cdot \frac{Q_{\text{out}}}{Q_{\text{in}}} \tag{2}$$

where N_{in} and N_{out} are the number of neutrons observed in the neutron detector during target-in and target-out runs, Q_{in} and Q_{out} are the time integrated beam currents as determined from the CT sensor, and B_{in} and B_{out} are experimentally determined background rates. The transmission coefficient T is calculated in bins of TOF, which are calibrated to bins in neutron kinetic energy.

target fill	live time (h)	after cuts (h)	Q	neutron events	selected neutrons	total ROI
Gas	2.7056e+08					
Liquid	1.1323e+08					

TABLE I. This table to be updated by Jingbo...

The neutron counts used in Eq. 2 are counts of neutron events which survive time-dependent run quality cuts and neutron selection cuts, as summarized in Table I. To minimize the impact of non-linearity between the CT sensor and the neutron beam intensity, the analysis only includes the 95% of collected data taken while the beam current was near the maximum value. Periods of instability in the data acquisition system, which were occassionally observed as a precipitous drop in neutron event rate while the beam current was constant, were also removed from the analysis. A dramatic decrease in the beam-intensity normalized neutron event rate was observed each time the dewars were filled with liquid argon. The rate returned to a plateau value during the 15-20 minute period that followed each filling. While filling the target, significant amounts of liquid argon vapor and gas would spill onto the brass collimators downstream of the target. We suspect that this caused the collimators to move out of alignment and then realign as the collimators returned to room temperature. We removed the 12% of liquid argon data from the periods during and following filling when the beam-current normalized neutron rate was less than 95% of the plateau value. Neutron selection cuts require both PMTs to register pulses within a 100 ns coincidence window, and to pass a cut which removes retriggered events.

BACKGROUND DETERMINATION

Determination of the argon transmission coefficient in Equation 2 relies on subtracting background events, both those arising from non-neutron sources, such as radiogenic background, and from neutrons (or secondary particles) with a measured TOF inconsistent with the neutron kinetic energy. Data collected while the beam was off indicates that beam independent background is negligible in the ROI. Data collected with the beam on but

a mechanical iron shutter closed before the flight path showed that background from the acellerator complex, such as skyshine or scattering from other experiments, is likewise neglible, as the resulting events arrive quite late, well outside of our ROI. The background from slow neutrons, which could alias as faster neutrons from a later pulse, is effectively eliminated by the addition of a 0.16 cm thick cadmium filter. The cadmium filter supresses neutrons with kinetic energy below 0.5 eV, and the remaining neutrons arrive reliably within the 50 ms between pulses.

The tight timing requirement significantly reduces background from random noise and PMT after pulsing.

Our 9 cm neutron detector is located about 30 m from the target, presenting a tiny solid angle for neutrons that might reach the detector through secondary scattering. Our analysis indicates that the major background contribution is consistent with neutrons which reach the near detector and undergo multiple scattering near the detector. The correlation between time-of-flight and neutron energy is lost for these events, and the resulting background is flat in TOF across our region of interest. To estimate the background B present in neutron counts N we run under identifical conditions apart from the insertion of a 2.5 cm thick aluminum filter into the beam-line. From the resulting neutron counts N_{Al} scaled to the same exposure as N we calculate the background as:

$$B = \frac{N_{\mathrm{Al}} - T_{\mathrm{Al}} \cdot N}{1 - T_{\mathrm{Al}}} \tag{3}$$

where T_{Al} is the known transmission coefficient of the aluminum filter, smeared by energy resolution. This technique [18] uses the narrow resonances near our region of interest in the neutron-aluminum cross section to provide a peek at the background. The amount by which count $N_{\mathrm{Al}}(E)$ in a narrow resonance exceeds the projected count from the known aluminum transmission $T{\cdot}N$ indicates the amount of background.

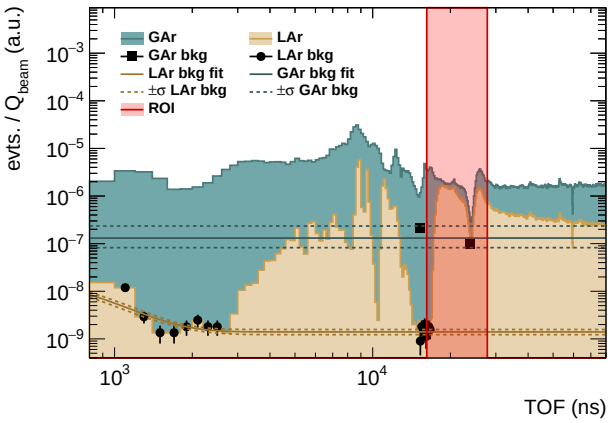

FIG. 1. Extraction of beam-related backgrounds.

As shown in Fig. 1, the background analysis is done in bins of TOF where the background is quite flat. The background differs for liquid and gas fills, as the neutrons reaching the detector at the end of the beam line differ by more than an order of magnitude. The statistically significant background estimates from Equation 3 are fit to an exponential and constant for liquid argon, and to a constant for gaseous argon. The exponential feature has neglible effect in the ROI. Overall the background contribution is $X\%$ for liquid argon and 2.64% for gaseous argon.

CALIBRATION

The neutron detector records a time-of-flight (TOF) which, when calibrated, determines the kinetic energy of each neutron event. Each neutron scatters inside the moderator for an unknown time. The average time spent in the moderator t_{mod} can be determined from the energy-dependent probability distribution, or moderator function, which has has been determined for the LANSCE facility by Monte Carlo simulation[25]. The velocity v of each neutron, and thus the kinetic energy E, is calculated from the measured TOF t as:

$$v(t) = \frac{L_{\mathrm{fit}}}{t - t_{\mathrm{mod}}(t) + t_{\mathrm{fit}}} \tag{4}$$

where L_{fit} and t_{fit} are parameters determined by fitting features in the collected TOF data to known resonances of aluminum and cadmium, both present in the beamline, and argon. The TOF-dependent moderator correction $t_{\mathrm{mod}}(t)$ is determined from the energy dependent correction using an iterative procedure.

In our energy ROI, the TOF for neutrons traversing the flight path varies by 9 μs, and the moderator correction is typically $1-2\%$. The best fit value of L_{fit} is 63.82 m which agrees well with physical measurements made along the beam line. The parameter t_{fit} accounts for time delays in the Li-glas detector, cables, and the DAQ system, as well as any residual difference between the actual and simulated moderator response.

The energy resolution is primary limited by the width of the moderator function $\sigma(t_{\mathrm{mod}}$ which is typically 10% of the TOF. The incident neutron pulse, which has a triangular shaped pulse with FWHM of 125 ns, contains 68% within $\sigma(t_0) = 53$ ns.

The use of gaseous argon fill during target out runs, instead of vacuum, is accounted for in the effective target number density:

$$n_{\mathrm{trg}} = n_{\mathrm{in}} - n_{\mathrm{out}} \tag{5}$$

where n_{in} is the argon number density for liquid argon fills and n_{out} is for gaseous argon fills. [Temperature and pressure of gaseous argon used?]

E (keV)	TOF (ns)	$\sigma(t_0)$ (ns)	$\pm\sigma(t_{\rm mod})$ (ns)	$\pm\Delta E/E$ (%)
30-40	24816	53	+334, -130	+2.7, -1.0
40-50	21861	53	+341, -146	+3.1, -1.3
50-60	19744	53	+313, -128	+3.1, -1.3
60-70	18134	53	+286, -120	+3.1, -1.3

TABLE II. Main sources of uncertainties in TOF contributing to the energy resolution. minor updated from Jingbo needed since removal of t_d.

The ARTIE vessel was held at atmospheric pressure, so the argon was continuously boiling during liquid fills. The number density $n_{\rm in}$ of the boiling liquid argon was measured directly in a separate experiment at UC Davis. The entire target assembly was placed on a precision scale, one of the argon dewars was instrumented with a stainless-steel ruler, and a video camera was arranged to simultaneously record the scale and ruler.

The scale was calibrated to detector volume by incrementally filling the vessel with known volumes of water, and the mass of the target apparatus was determined when the vessel was filled with air. The target was filled with liquid argon, and recorded during the boil off period. To avoid measurement instability resulting from large bubbles emerging from the dewar, our analysis excludes volume readings which were not stable to within 25 mL for a 1 second time interval. The detector volume as function of time was linear with a measured boil-off rate of 1.56 L/hr, consistent with our filling rate of 1.5 to 2.0 L/hr while conducting the experiment. The effective target density was determined to be $n_{\rm in} = 1.318 \pm 0.017$ kg/L. The analysis included corrections for the thermal expansion of the target vessel, the additional weight from ice forming on the window, and the difference in altitute between UC Davis and Los Alamos. [How was uncertainty determined?]

Despite being flushed continuosly with dry nitrogen gas, the kapton [text originally said mylar?] windows located at each end of the target developed a thin layer of ice during liquid argon runs. Once the ice buildup reached ~ 5 mm, the target was warmed up to melt the ice. The transmission coefficient for the ice at its maximum thickness was determined from Eq. 2 with runs taken immediately before each warm-up, with maximal ice build-up, used as "target in", and runs taken immediately after the warm-up, with minimal ice build-up, used as "target out". A Monte Carlo simulation was used to determine the transmission coefficient of ice using the incident neutron spectrum and the ENDF total cross section. The best-fit ice thickness was found to be $d = 0.030^{+0.095}_{-0.025}$ cm, which is consistent with our observation that 5 mm ice powder consisted of ice crystals mixed with a significant amount of air.

SYSTEMATIC UNCERTAINTIES

name	affected parameters	parameter uncertainty	cross section uncertainty
beam instability	$Q_{\rm in}, Q_{\rm out}$	$\pm$1.0%	$\pm$1.0%
thermal misalignment	$Q_{\rm in}$	-5%	-3.1%
boiling	$n_{\rm in}$	$\pm$1.3%	$\pm$1.3%
ice buildup	$Q_{\rm in}$	-3.8%	-2.4%
atmospheric pressure	$n_{\rm eff}$	$\pm$0.4%	$\pm$0.4%
target-in background	$B_{\rm in}$		
target-out background	$B_{\rm out}$		

TABLE III. Summary of systematic uncertainties. updated needed from Mike

The stability of the beam, beam monitoring, target alignment, and neutron detector efficiency was assessed during special runs during which the target vessel contained air. An analysis of the average neutron rate during two days of running at the start the experiment and one day of running at the end showed that these systematic effects remained within 1.1%.

The event selection removes the time period immediately following each liquid argon fill during which the observed neutron rate was less than 95% of the plateau rate. We assess a one-sided -5% systematic uncertainty which we attribute to transient inadvertent thermal misalignment of the collimators after each fill.

The number density of boiling liquid argon in the target was experimentally determined with an associated systematic uncertainty of 1.3%. [I took this from 0.17/1.318.. differs from value in the table of 1.5% How was this uncertainty determined?]

The measured cross section was not corrected for ice buildup on the kapton windows. Instead, the simulated transmission coefficient for ice with a thickness equal to the 1 sigma upper bound on experimentally determined maximum ice thickness (1.3cm) is taken as a one-sided systematic uncertainty (-3.8%) on the beam intensity.

The last 2 m of the flight path is housed in a non-temperature controlled building. During the course of the data taking, the average air density was found to be 0.85 mg/cm^3 with a maximum of 0.95 mg/cm^3 and a minimum of 0.75 mg/cm^3, using data collected from the TA-53 (LANSCE) and TA-54 (White Rock) weather stations. The maximum variation in the neutron flux reaching the detector was calculated from the maximum variation in the air density and the known cross section for the three main constituents of air. The variation 0.4% was applied as a systematic due to atmospheric pressure.

After our selection cuts, several systematic uncertainties were determined to be neglible, including those from: non-linearity between the beam intensity and CT measurement, dead time in the data acquisition system, PMT afterpulsing, and contamination of the argon gas.

The absolute energy calibration is limited by the statis-

tical uncertainties on the fitted parameter $\sigma(t_{\rm fit}) = 29$ ns, and the contribution from $\sigma(L_{\rm fit}) = 0.064$ m is neglible. No systematic uncertainty for energy resolution is applied to the cross section results, which are reported as function of measured energy.

CONCLUSIONS

From the experimentally determined neutron counts in each TOF bin, the transmission coefficient T is calculated from Eq. 2 and the cross section from Eq. 1. The central value of each TOF bin is coverted to energy using Eq 4, which determines the kinetic energy dependence of these experimentally determined quantities.

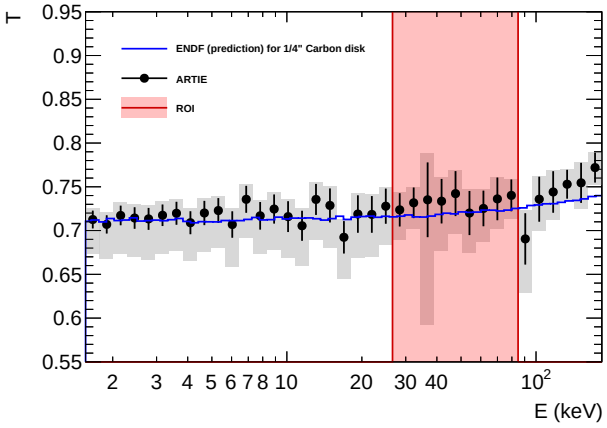

FIG. 2. Transmission coefficient T obtained for two 0.125 ± 0.010 thick carbon (99.999% purity) disk inserted in the beam line attached to the ARTIE target. Good agreement (χ^2/NDF $= 2.7/6 = 0.45$ in the ROI) is found with the theoretical prediction of T obtained using the carbon cross section tabulated in ENDF and smeared by the measured energy resolution of ARTIE.

As a cross check of the experimental methods and analysis procedure, the cross section of carbon was determined from data collected with two 0.125 ± 0.010 thick carbon (99.999% purity) disks [28] attached to the ARTIE target while it was flushed with gaseous argon. Fig. 2 shows the measured transmission coefficient $T(E)$ as a function of the energy compared to the theoretical prediction from ENDF smeared by the detector energy resolution. Good agreement (χ^2/NDF $= 2.7/6 = 0.45$ in the ROI) was found.

The measured neutron-argon total cross section as a function of kinetic energy is shown in Fig. 3. Our results are consistent with the prediction from the ENDF cross section smeared by the ARTIE energy resolution for the range from 40 to 70 keV. In the region from 30 to 40 keV our results reproduce the EXFOR results which differ from the ENDF prediction. [In addition, at 35 keV aluminum also has a large resonance (34 barns) that limits statistics, as the vacuum beam pipe flanges are made of aluminum.] The EXFOR experiment was optimized for a scan of a much wider energy region and higher cross section, and our results only differ for cross sections less than 0.2 b. We suspect that our results are consistent if statistical uncertainty of the EXFOR results in the regions of low cross section are accounted for. Our results confirm the predicted anti-resonance feature at 57 keV, which has profound implications on the ability of neutrons to traverse large distances in liquid argon detectors and shielding.

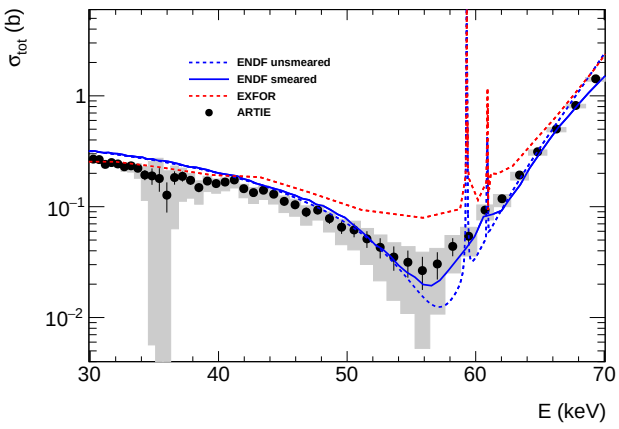

FIG. 3. Neutron-argon total cross section as a function of energy

ACKNOWLEDGEMENTS

This work was supported by the U.S. Department of Energy (DOE) Office of Science under award number DE-SC0009999, and by the DOE National Nuclear Security Administration through the Nuclear Science and Security Consortium under award number DE-NA0003180. This work was supported by the U.S. Department of Energy through the Los Alamos National Laboratory. Los Alamos National Laboratory is operated by Triad National Security, LLC, for the National Nuclear Security Administration of U.S. Department of Energy (Contract No. 89233218CNA000001). We gratefully acknowledge the logistical and technical support and the access to laboratory infrastructure provided to us by LANSCE and its personnel.

BIBLIOGRAPHY

[1] M. Antonello et al. ICARUS at FNAL. 2013.

[2] R. Acciarri et al. Design and Construction of the MicroBooNE Detector. *JINST*, 12(02):P02017, 2017.

[3] B. Abi et al. The Single-Phase ProtoDUNE Technical Design Report. 2017.

[4] R. Acciarri et al. Long-Baseline Neutrino Facility (LBNF) and Deep Underground Neutrino Experiment (DUNE) Conceptual Design Report, Volume 4 The DUNE Detectors at LBNF. 2016.

[5] C. E. Aalseth et al. DarkSide-20k: A 20 tonne two-phase LAr TPC for direct dark matter detection at LNGS. *Eur. Phys. J. Plus*, 133:131, 2018.

[6] K. H. Ackermann et al. The GERDA experiment for the search of $0\nu\beta\beta$ decay in ^{76}Ge. *Eur. Phys. J.*, C73(3):2330, 2013.

[7] N. Abgrall et al. The Large Enriched Germanium Experiment for Neutrinoless Double Beta Decay (LEGEND). *AIP Conf. Proc.*, 1894(1):020027, 2017.

[8] A.F. Michaudon and S.A. Wender. Performance of the lansce wnr facility as an intense pulsed neutron source for neutron nuclear physics. Report LA-UR-90-4355, LANSCE, 1990.

[9] Heil, M. and others. A 4π BaF_2 detector for (n,γ) cross section measurements at a spallation neutron source. *Nucl. Instrum. Meth.*, A459:229–246, 2001.

[10] S. Mosby, F. Tovesson, A. Couture, D.L. Duke, V. Kleinrath, R. Meharchand, K. Meierbachtol, J.M. ODonnell, B. Perdue, D. Richman, and D. Shields. A fission fragment detector for correlated fission output studies. *Nuclear Instruments and Methods in Physics Research Section A: Accelerators, Spectrometers, Detectors and Associated Equipment*, 757:75 – 81, 2014.

[11] C. D. Nesaraja and E. A. McCutchan. Nuclear Data Sheets for A = 41. *Nucl. Data Sheets*, 133:1–220, 2016.

[12] S. Agostinelli et al. Geant4 - a simulation toolkit. *Nuclear Instruments and Methods in Physics Research Section A: Accelerators, Spectrometers, Detectors and Associated Equipment*, 506(3):250 – 303, 2003.

[13] J. Allison et al. Recent developments in Geant4. *Nuclear Instruments and Methods in Physics Research Section A: Accelerators, Spectrometers, Detectors and Associated Equipment*, 835:186 – 225, 2016.

[14] D. A. Brown et al. ENDF/B-VIII.0: The 8th Major Release of the Nuclear Reaction Data Library with CIELO-project Cross Sections, New Standards and Thermal Scattering Data. *Nucl. Data Sheets*, 148:1–142, 2018.

[15] C.H. Westcott and Atomic Energy of Canada Limited. *Effective Cross Section Values for Well-moderated Thermal Reactor Spectra*, volume 41 of *AECL (Series)*. Atomic Energy of Canada, 1970.

[16] M. Wang, G. Audi, F. G. Kondev, B. Pfeiffer, J. Blachot, X. Sun, and M. MacCormick. NUBASE2012 Evaluation of Nuclear Properties. *Nucl. Data Sheets*, 120:6–7, 2014.

[17] John Cameron, Jun Chen, Balraj Singh, and Ninel Nica. Nuclear Data Sheets for A = 37. *Nucl. Data Sheets*, 113:365–514, 2012.

[18] J.M. Brown, A. Youmans, N. Thompson, Y. Danon, D.P. Barry, G. Leinweber, M.J. Rapp, R.C. Block, and R. Bahran. Neutron Transmission Measurements and Resonance Analysis of Molybdenum-96. *AccApp '17*, 2017.

[19] R. Ajaj et al. Search for dark matter with a 231-day exposure of liquid argon using DEAP-3600 at SNOLAB. *Phys. Rev. D*, 100:022004, 2019.

[20] V. Fischer, L. Pagani, L. Pickard, C. Grant, J. He, E. Pantic, R. Svoboda, J. Ullmann, and J. Wang. Absolute Calibration of the DANCE Thermal Neutron Beam using Sodium Activation. *Nucl. Inst. and Meth. A*, 929:97, 2019.

[21] V. Fischer, L. Pagani, L. Pickard, C. Grant, J. He, E. Pantic, R. Svoboda, J. Ullmann, and J. Wang. Measurement of the Neutron Capture Cross Section on Argon. *Phys. Rev. D*, 99:103021, 2019.

[22] R.R. Winters, R.F. Carlton, C.H. Johnson, F.W. Hill, and M.R. Lacerna. Total cross section and neutron resonance spectroscopy for $n + ^{40}Ar$. *Phys. Rev. C*, 43:492, 1991.

[23] M.S. Moore. Rate dependence of counting losses in neutron time-of-flight measurements. *Nucl. Inst. and Meth.*, 169:245, 1980.

[24] D.A. Brown et al. Endf/b-viii.0: The 8th major release of the nuclear reaction data library with cielo-project cross sections, new standards and thermal scattering data. *Nucl. Data Sheets*, 148, 2018.

[25] Lukas Zavorka, Michael J. Mocko, Paul E. Koehler, and John L. Ullmann. Benchmarking of the MCNPX Predictions of the Neutron Time-emission Spactra at LANSCE. American Nuclear Society, 20th Topical Meeting of the Radiation Protection and Shielding Division of ANS, 2018.

[26] H.M. Roder. Liquid densities of oxygen, nitrogen, argon, and parahydrogen. *NBS Technical Note 361 (Revised)*, 1974.

[27] B.J.P. Jones et al. *JINST*, 8, 2013.

[28] Carbon (graphite) (c) sputtering targets. `https://www.lesker.com/newweb/deposition_materials/depositionmaterials_sputtertargets_1.cfm?pgid=car1`.